Enhancement of superconductivity and suppression of charge-density wave in As-doped CsV_3Sb_5

Yi Liu,[1,2,*] Chang-Chao Liu,[1] Qin-Qing Zhu,[1,3] Liang-Wen Ji,[1] Si-Qi Wu,[1] Yun-Lei Sun,[4] Jin-Ke Bao,[5] Wen-He Jiao,[6] Xiao-Feng Xu,[6] Zhi Ren,[3] and Guang-Han Cao[1,7,†]

[1]*School of Physics, Zhejiang Province Key Laboratory of Quantum Technology and Devices, Zhejiang University, Hangzhou 310058, China*

[2]*Department of Applied Physics, Key Laboratory of Quantum Precision Measurement of Zhejiang Province, Zhejiang University of Technology, Hangzhou 310023, China*

[3]*School of Science, Westlake Institute for Advanced Study, Westlake University, Hangzhou 310064, China*

[4]*School of Information and Electrical Engineering, Zhejiang University City College, Hangzhou 310015, China*

[5]*Department of Physics, Materials Genome Institute and International Center for Quantum and Molecular Structures, Shanghai University, Shanghai 200444, China*

[6]*Department of Applied Physics, Zhejiang University of Technology, Hangzhou 310023, China*

[7]*Collaborative Innovation Centre of Advanced Microstructures, Nanjing University, Nanjing 210093, China*

(Received 4 August 2022; accepted 21 November 2022; published 13 December 2022)

We have investigated the As-doping effect in the newly discovered kagome superconductor CsV_3Sb_5 via measurements of x-ray diffraction, electrical resistivity, magnetic susceptibility, and specific heat. Our results show that partial substitution of Sb with As leads to shrinkage of the *c* lattice, which effectively applies a chemical pressure in the system. The solubility of As atoms is about 2.3% for single crystals grown by the self-flux method. In the As-doped single crystal $CsV_3(Sb_{0.977}As_{0.023})_5$, the charge-density-wave (CDW) transition temperature T_{CDW} is suppressed from 94 to 83 K, and the superconducting transition temperature T_c is enhanced from 2.5 to 3.6 K. Furthermore, the residual resistivity ratio is significantly reduced, and the magnetoresistance with magnetic field along the *c* axis decreases by nearly one order of magnitude, indicating substantial disorder scattering induced by the As doping. The anomalous Hall effect (AHE) is only observed below T_{CDW}, indicating the intimate relationship between CDW and AHE. We found that the As-doping effect on T_c and T_{CDW} is basically equivalent to the hydrostatic pressure effect at 0.2 GPa.

DOI: 10.1103/PhysRevMaterials.6.124803

I. INTRODUCTION

Recently, the newly discovered kagome metals AV_3Sb_5 (A = K, Rb, Cs) [1] have attracted a great deal of attention for their novel properties, including superconductivity (SC) [2–4], unconventional chiral charge-density wave (CDW) [5–14], and nontrivial band topology [15,16]. AV_3Sb_5 crystalizes in a quasi-two-dimensional lattice consisting of alternating A^+ and $(V_3Sb_5)^-$ slabs. As shown in Fig. 1(a), the V cations make up a kagome net with in-plane Sb1 atoms on the centers of hexagons, and the Sb2 atoms form a honeycomb lattice at both sides. The superconducting transition temperatures, T_c, for A = K, Rb, and Cs are 0.93, 0.92, and 2.5 K, respectively. Various measurements focusing on the superconducting state have revealed multigap *s*-wave SC in CsV_3Sb_5 [17–20]. The first-principles calculations show that the electronic states near the Fermi level are contributed mainly from the V-3*d* and Sb-5*p* states and there are several bands crossing the Fermi surface. At the *M* point, hole bands with weak dispersions form the saddle points, which contribute the time-reversal and inversion symmetry-protected Dirac quasiparticles [15,16,21]. The angle-resolved photoemission spectroscopy together with density functional calculations revealed multiple van Hove singularities near the Fermi surface [22]. These van Hove singularities are considered to induce Fermi surface instability and drive the CDW transition. As suggested by Jiang *et al.* [5], this charge order is responsible for the giant unconventional anomalous Hall effect (AHE) observed below T_{CDW} [23,24], and it also opens up the possibility of unconventional SC in this system. Thus, AV_3Sb_5 provides an ideal platform to explore the interplay between SC, CDW, and nontrivial topology.

One of the most interesting interplays is the competition between the SC and the CDW. Applying pressure is an effective method to tune the different electronic states. Under hydrostatic pressures, SC and CDW present an intimate and complicated relationship [25–30]. As the CDW is suppressed monotonously with increasing pressure, the superconducting transition temperature experiences two maxima, and the second peak coincides with the vanishing of the CDW. Note that a double superconducting dome is usually observed in unconventional superconductors [31]. In CsV_3Sb_5, the two superconducting domes are supposed to have different charge orders. The low-pressure dome originates from the suppression of the CDW, while the second dome may be related to the pressure-induced Lifshitz transition [25,28]. Nevertheless, these novel superconducting states appear only under high pressures, which is unfavorable for in-depth studies. The other

*liuyiphy@zjut.edu.cn
†ghcao@zju.edu.cn

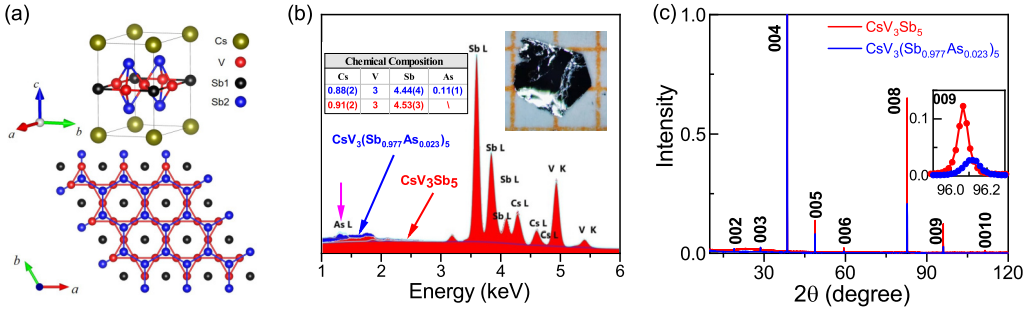

FIG. 1. (a) Crystal structure of CsV_3Sb_5. (b) Comparison of EDX spectra highlighting the signal from As atoms. (c) XRD patterns for the crystals of CsV_3Sb_5 and $CsV_3(Sb_{0.977}As_{0.023})_5$. The (009) peaks are magnified to show the shift.

method is chemical doping. In CsV_3Sb_5, since the van Hove singularities are just below the Fermi level, hole doping is expected to drive the van Hove singularities closer to the Fermi level. Extra holes could be introduced by doping at different atom sites. In the case of Cs deficiency, realized by selective oxidation [32], a superconducting dome was revealed accompanied by the suppression of the CDW. In Ti doping at V sites and Sn doping at Sb sites, the CDW is suppressed rapidly, and T_c presents two domes as a function of the effective doping [33,34]. Additionally, for partial substitution of Sb with Sn, the Sn atoms have the chance to enter either Sb1 or Sb2 sites, which brings different effects on the electronic structure. The room-temperature nuclear quadrupole resonance measurements revealed that the Sn preferred to occupy the Sb1 site. The first-principles calculations showed that external hydrostatic pressure and hole doping shifted the location of van Hove singularities in a contrary way, and therefore it affected the electronic orders differently [35]. For isovalent doping with partial substitution of V with Nb in CsV_3Sb_5, negative chemical pressure and disorder are introduced, accompanied by the suppression of the CDW and enhancement of SC [36]. The DFT-based calculation and angle-resolved photoemission spectroscopy experiment reveal an antiphase shift of Fermi energy with respect to M and Γ points [36,37]. Is it possible to generate a positive chemical pressure similar to external hydrostatic pressure in the system through an isovalent chemical doping?

Here we report on the "chemical pressure" effect by substituting part of Sb atoms with As atoms in CsV_3Sb_5. Different from the negative chemical pressure induced by Nb doping, As doping is expected to introduce positive chemical pressure, reminiscent of P doping in iron-based superconductors [38]. In this paper, we successfully grew As-doped single crystals by the self-flux method. Compared with CsV_3Sb_5, the lattice parameter is indeed shortened, with the T_{CDW} decreased by 11 K, and T_c increased by 44%. The specific heat, anisotropic upper critical field, magnetoresistivity, and AHE are also measured and discussed.

II. EXPERIMENTAL METHODS

Single crystals of $CsV_3(Sb_{1-x}As_x)_5$ were grown by spontaneous nucleation with the self-flux method [1]. First, the elements of Cs, V, Sb, and As were mixed in a molar ratio of $10 : 3 : 30(1-x) : 30x$ with a total mass of about 3 g. The mixtures were loaded in an alumina crucible, which was then jacketed in a Ta tube. The Ta tube was welded through argon arc melting and sealed in an evacuated quartz ampoule. Subsequently, the sample-loaded quartz ampoule was heated up to 920 °C holding for 1000 min in a muffle furnace, followed by cooling down to 500 °C at a rate of 2 °C/h. The obtained crystals were embedded in the flux, which was washed off by ethanol. Shiny platelike crystals with a typical size of $2 \times 2 \times 0.1$ mm^3 were harvested, as shown in the inset of Fig. 1(b). As-doped polycrystals with higher doping levels have also been attempted, and an impurity phase VAs_2 appeared when the As content was higher than 3%. The composition of the As-doped crystals was determined by energy-dispersive x-ray spectroscopy (EDS) on a scanning electron microscope (Hitachi S-3700N) equipped with an Oxford Instruments X-Max spectrometer. X-ray diffraction (XRD) was carried out on a PANalytical x-ray diffractometer (Model EMPYREAN) with monochromatic Cu $K\alpha 1$ radiation at room temperature. Electrical transport and heat capacity measurements were conducted on a Quantum Design physical property measurement system (PPMS-9). The longitudinal resistivity and Hall resistivity were measured with a four-electrode method on strip-shaped and square sheets, respectively. The heat capacity measurement was performed using the thermal relaxation method. The magnetization measurements were performed on a SQUID magnetometer (MPMS-5).

III. RESULTS

Single crystals of $CsV_3(Sb_{1-x}As_x)_5$ with a nominal doping level of x from 1% to 5% were grown using the above method. Unexpectedly, with the increase of As content, extra crystals of VAs appear and the actual doping level tends to saturate. The elemental compositions of the nondoped and As-doped crystals are both determined by EDS measurements for comparison. Although the signal from the As element is weak, by comparing with the EDS of CsV_3Sb_5, the spectrum corresponding to the As element is evident, as shown in Fig. 1(b). The As content of different crystals from the batch with $x = 0.03$ ranges from 2.1% to 2.4%, indicating good compositional homogeneity. The average value of As content measured is $x = 2.3\%$, slightly lower than the nominal value. We note that the Cs and Sb contents are slightly off the stoichiometric ratio for both crystals of CsV_3Sb_5 and $CsV_3(Sb_{0.977}As_{0.023})_5$, which may come from systematic measurement errors.

The XRD patterns for single crystals of CsV_3Sb_5 and $CsV_3(Sb_{0.977}As_{0.023})_5$ are shown in Fig. 1(c). To eliminate the effect of zero shift, a very thin layer of Si powder was coated on the surface as an internal standard. Only (00l) reflections are observable here, indicating that the c orientation of the crystals is perpendicular to the crystal plate. The (00l) reflections shift to higher angles for the As-doped crystals, as shown in the inset of Fig. 1(c). Indeed, the c parameters, calculated by a least-squares fit, are 9.328(4) and 9.313(2) for CsV_3Sb_5 and $CsV_3(Sb_{0.977}As_{0.023})_5$, respectively. Namely, the c axis for the As-doped crystal is shortened by 0.16%, suggesting that the isovalent substitution of Sb with As has effectively generated pressure to the system. The decrease of the c parameter is consistent with the results of hydrostatic pressure [28,39]. Estimated from the lattice shrinkage, the corresponding hydrostatic pressure in $CsV_3(Sb_{0.977}As_{0.023})_5$ is about 0.1 GPa through linear extrapolation [28].

Figures 2(a) and 2(b) show the temperature dependence of magnetic susceptibility under magnetic fields of 1 mT and 1 T with the direction parallel to the ab plane for CsV_3Sb_5, $CsV_3(Sb_{0.981}As_{0.019})_5$, and $CsV_3(Sb_{0.977}As_{0.023})_5$. Crystal of $CsV_3(Sb_{0.981}As_{0.019})_5$ is selected from the batch with a nominal doping level of 2%, and EDS measurement reveals that the actual doping level is about 1.9%. The low-field data exhibit a strong diamagnetism at low temperatures, demonstrating SC. The volume fractions of magnetic shielding approach ~90% at 1.8 K, indicating bulk SC. For the undoped CsV_3Sb_5, SC occurs at 2.5 K, in accordance with previous reports [16,17,24]. For samples of $CsV_3(Sb_{0.977}As_{0.019})_5$ and $CsV_3(Sb_{0.977}As_{0.023})_5$, SC appears at T_c = 3.3 and 3.6 K, respectively. The superconducting transition temperature is increased by as much as 44% in $CsV_3(Sb_{0.977}As_{0.023})_5$.

In the broad temperature range above SC, the susceptibility shows a sudden decrease of susceptibility at T_{CDW} = 94, 86, and 83 K for CsV_3Sb_5, $CsV_3(Sb_{0.977}As_{0.019})_5$, and $CsV_3(Sb_{0.977}As_{0.023})_5$, respectively. Above T_{CDW}, the susceptibility is nearly independent of temperature, indicating Pauli paramagnetism. The susceptibility tail at low temperatures is attributed to tiny unknown paramagnetic impurities/defects. To investigate the changes in physical properties caused by As doping, the crystal with the relatively high doping level, namely $CsV_3(Sb_{0.977}As_{0.023})_5$, is chosen for detailed measurements and discussions in the following section. The Pauli susceptibility, χ_P, defined as the value of susceptibility at 300 K [40], is 3.6×10^{-4} and 3.3×10^{-4} emu mol^{-1} Oe^{-1} for CsV_3Sb_5 and $CsV_3(Sb_{0.977}As_{0.023})_5$, respectively. The Pauli paramagnetic susceptibility is proportional to the density of states (DOS) near the Fermi level with $\chi_P = \mu_B^2 D(E_F)$, where μ_B is the Bohr magneton. Therefore, the corresponding DOSs are 11.4 and 10.5 eV^{-1} f.u.$^{-1}$, which is consistent with the result of DFT calculation (10 eV^{-1} f.u.$^{-1}$) in CsV_3Sb_5 [16]. Furthermore, the CDW-induced reductions of the DOS, calculated from the changes of susceptibility $\Delta\chi$, are 1.0 and 0.5 eV^{-1} f.u.$^{-1}$ for CsV_3Sb_5 and $CsV_3(Sb_{0.977}As_{0.023})_5$, respectively. The drops of susceptibility at the CDW transition reduce by half, indicating significant suppression of CDW order in $CsV_3(Sb_{0.977}As_{0.023})_5$.

Figure 3 shows the temperature dependence of in-plane resistivity for the $CsV_3(Sb_{0.977}As_{0.023})_5$ crystal. The resistivity in the normal state is about 6.0 $\mu\Omega$ cm at 5 K, much larger

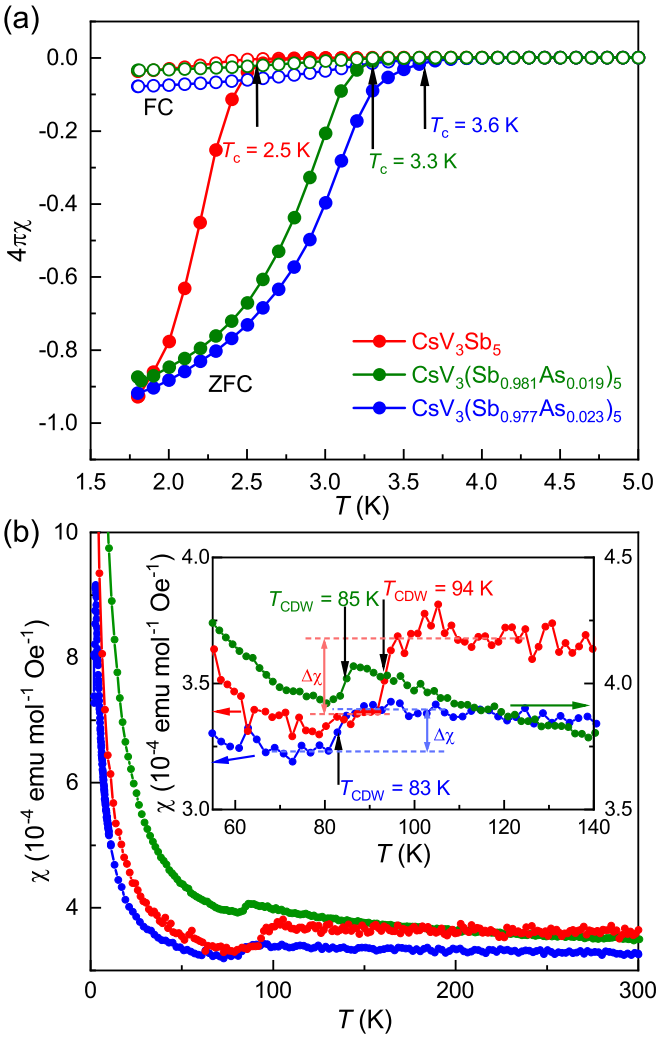

FIG. 2. (a) The low-temperature susceptibility for CsV_3Sb_5, $CsV_3(Sb_{0.981}As_{0.019})_5$, and $CsV_3(Sb_{0.977}As_{0.023})_5$ in ZFC (solid symbols) and FC (open symbols) modes under 1 mT with magnetic field parallel to the ab plane. (b) Temperature dependence of magnetic susceptibility at 1 T. The inset is the closeup of the CDW transitions, and $\Delta\chi$ is labeled as the change of susceptibility.

than the corresponding value of CsV_3Sb_5 (~1.0 $\mu\Omega$ cm, consistent with other reports [16,17,24]). Meanwhile, the residual resistivity ratio (RRR) decreases from 69 to 16, indicating the disorder scattering from the As doping. The low-temperature data (from 5 to 50 K) are fitted with the formula $\rho(T) = \rho_0 + AT^2$. The fitted A values are 2.88 and 4.08 nΩ cm K^{-2} for CsV_3Sb_5 and $CsV_3(Sb_{0.977}As_{0.023})_5$, respectively. The A value is related to the correlation of quasiparticles, and we will come back to it in the discussion part. At low temperatures, the superconducting transition appears below T_c^{onset} = 3.91 K. At T_c^{mid} = 3.6 K, the resistivity drops to half of the residual resistivity. The transition width, defined by the temperature difference between T_c^{onset} and T_c^{offset}, is about 0.6 K, indicting good homogeneity of the sample. The above result is consistent with the magnetic measurement, in which T_c is defined by the appearance of diamagnetism in susceptibility. At high temperatures, a CDW-induced kinklike anomaly

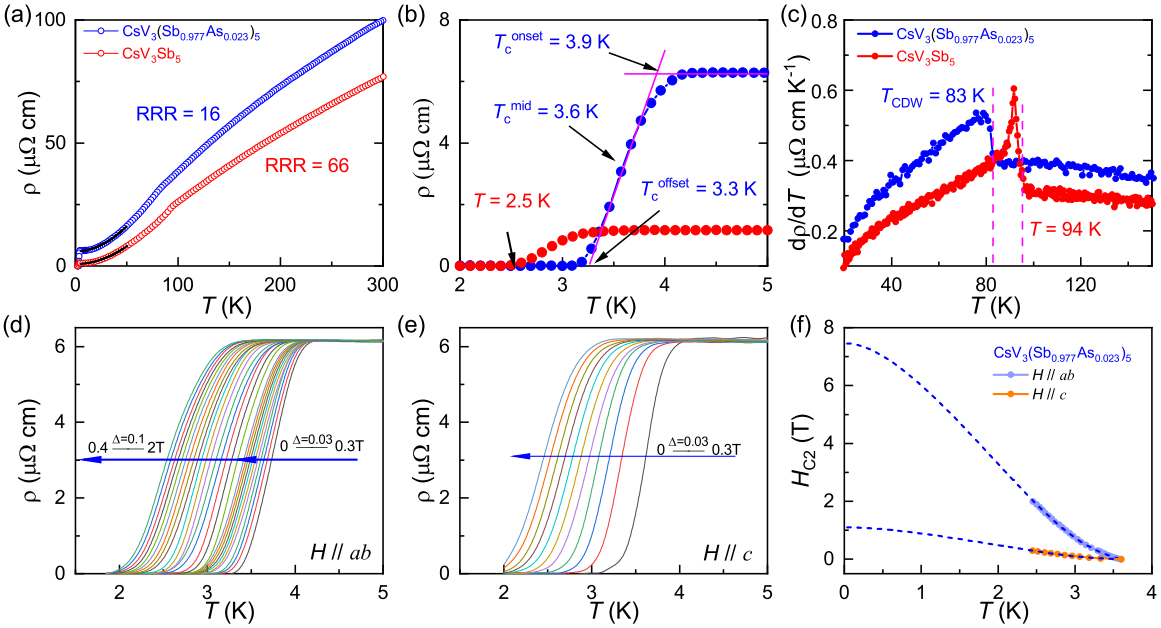

FIG. 3. (a) Temperature dependence of resistivity for CsV_3Sb_5 and $CsV_3(Sb_{0.977}As_{0.023})_5$. The solid black lines are the quadratic fitting from 5 to 50 K. (b) Amplification around the superconducting transition. (c) The derivative of resistivity around the CDW transition. (d) The superconducting transitions under magnetic fields perpendicular to the c axis. The field intervals are 0.03 and 0.1 T, respectively, for $B < 0.3$ T and $0.3 < B < 2$ T. (e) The superconducting transitions under magnetic fields along the c axis. The field is up to 0.3 T with an interval of 0.03 T. (f) Temperature dependence of anisotropic upper critical field for CsV_3Sb_5 and $CsV_3(Sb_{0.977}As_{0.023})_5$. The dashed green line is the fitting based on the two-band model.

appears at around 83 K, which is observed more clearly in $d\rho/dT$, as shown in Fig. 3(c). This anomaly is also consistent with the appearance of a drop in high-field susceptibility. The measurements under a hydrostatic pressure of 0.19 GPa [27] or 0.36 GPa [41] showed a CDW transition at about 83 K, accompanying with T_c^{mid} at about 3.2 K. Except for the pressure effect, the disorder induced by As substitution may also move the saddle point away from the Fermi level, similar to the case reported in Nb-doped CsV_3Sb_5 [36,37], in which the isovalent Nb doping also suppresses the CDW and enhances SC gradually.

Figures 3(d) and 3(e) show the superconducting transition under various magnetic fields parallel to the ab plane and the c axis, respectively. As expected, the T_c shifts to lower temperature with increasing magnetic field. By choosing 50% normal-state resistivity as the criterion to determine the $T_c(H)$, we obtained the temperature dependence of the upper critical field $H_{c2}(T)$, as presented in Fig. 3(f). The $H_{c2}(T)$ can be well-fitted by the equation proposed by Gurevich for two-band superconductors [42]. The $H_{c2}(0)$ values for magnetic field parallel and perpendicular to the ab plane are estimated to be $H_{c2}^{\parallel}(0) = 7.50$ T and $H_{c2}^{\perp}(0) = 1.1$ T, respectively. Both of them are slightly larger than the values in CsV_3Sb_5 [4], while the anisotropic ratio of the upper critical field $\eta = H_{c2}^{\parallel}(0)/H_{c2}^{\perp}(0)$ decreases from 9.0 to 6.8. For $CsV_3(Sb_{0.977}As_{0.023})_5$, the extra impurity scattering, which leads to the decrease of the mean free path and coherence length, will increase the upper critical field [43]. The η value is decreased by a quarter, clearly indicating weaker anisotropy in $CsV_3(Sb_{0.977}As_{0.023})_5$, which possesses a smaller interlayer distance.

Figure 4(a) shows the temperature dependence of specific heat $C(T)$ for $CsV_3(Sb_{0.977}As_{0.023})_5$. The specific heat at high temperature saturates at around the Dulong-Petit limit of $3NR = 224$ J K^{-1} mol^{-1}, where the N is the number of atoms per formula unit, and R is the gas constant. A peak induced by the CDW transition is observed at around $T_{CDW} = 83$ K. Figure 4(b) shows the plot of C/T versus T^2, which can be well fitted by the formula $C/T = \gamma + \beta T^2$, where γ is the Sommerfeld coefficient, corresponding to the contribution from itinerant electrons to specific heat, and β is related to the phonon contribution. The linear fit gives $\gamma = 16.77$ mJ K^{-2} mol^{-1}, which is larger than the value estimated from the Pauli paramagnetic susceptibility, $\gamma_{cal} = \frac{1}{3}\pi^2 k_B^2 \mu_B^2/\chi_P = 7.8$ mJ K^{-2} mol^{-1}. The γ value increases under the effect of electron-phonon or electron-electron interactions, suggesting the existence of quasiparticle interactions. The fitted β value is 4.95 mJ K^{-4} mol^{-1}, from which the Debye temperature θ_D is calculated to be 153 K using the formula $\theta_D = (\frac{12\pi^4}{5\beta} NR)^{1/3}$. With the Debye temperature, the electron-phonon coupling constant λ_{ep} is obtained using the McMillan equation [44]:

$$\lambda_{ep} = \frac{1.04 + \mu^* \ln\left(\frac{\theta_D}{1.45 T_c}\right)}{(1 - 0.62\mu^*)\ln\left(\frac{\theta_D}{1.45 T_c}\right) - 1.04}, \quad (1)$$

where the μ^* is the Coulomb pseudopotential parameter with a typical value of 0.13. The λ_{ep} values for CsV_3Sb_5 (calculated with the β value of 3.31 mJ K^{-4} mol^{-1} [17], corresponding to the $\theta_D = 174$ K) and $CsV_3(Sb_{0.977}As_{0.023})_5$ are 0.62 and 0.72, respectively, suggesting the moderate electron-phonon interaction in this system. The results are close to the

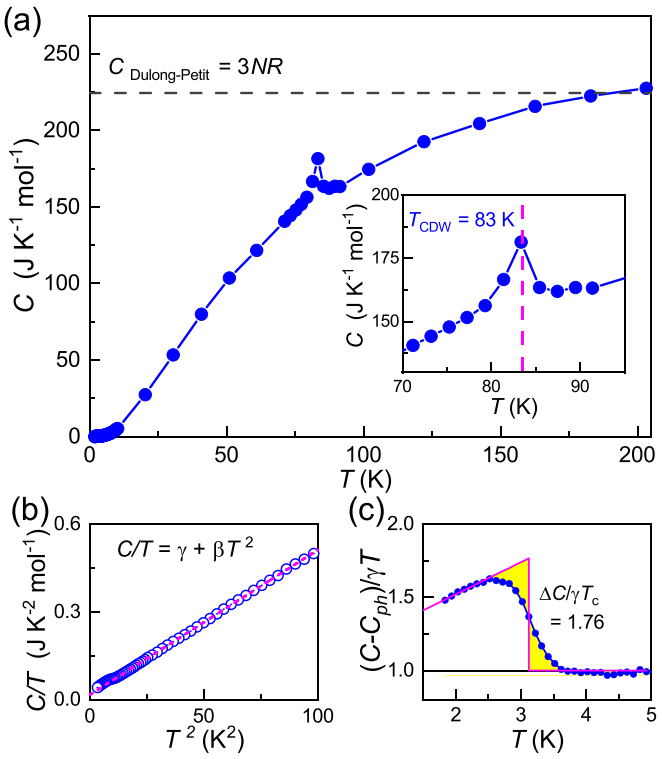

FIG. 4. (a) Temperature dependence of specific heat for $CsV_3(Sb_{0.977}As_{0.023})_5$. The inset shows the specific-heat peak related to the CDW at T_{CDW}. (b) Plot of C/T vs T^2 below 10 K. The dotted line is the linear fit above SC. (c) The specific-heat contribution from SC by subtracting the phonons part.

recent results of $\lambda_{ep} = 0.45$–0.6 measured by angle-resolved photoemission spectroscopy [45] and much larger than the value of 0.25 from the DFT calculations [9]. By subtracting the contribution from the phonon, the electronic specific heat C_e below 5 K is plotted using $C_e/(\gamma T)$ and T as the coordinates in Fig. 4(c). A jump corresponding to the superconducting transition starts at 3.6 K, coincident with the temperature of the onset of diamagnetism. The superconducting specific-heat jump $\Delta C^{(T=T_c)}/\gamma T_c \sim 1.76$, further confirming bulk SC in $CsV_3(Sb_{0.977}As_{0.023})_5$. The value is somewhat larger than the theoretical value 1.43 for a conventional BCS superconductor in the weak-coupling limit.

The quantum oscillations of isothermal magnetoresistance are expected to provide information about the electronic structure. Here, the field dependence of magnetoresistance (MR) under different temperatures with field along two directions, i.e., $H \parallel c$ and $H \perp c$, are presented in Figs. 5(a) and 5(b). Interestingly, the large MR and Shubnikov–de Haas quantum oscillations, which were observed in CsV_3Sb_5 at low temperatures with field along the c axis, are significantly suppressed in As-doped CsV_3Sb_5. Interesting, the curvature of MR at low field can be satisfactorily scaled to the curve of CsV_3Sb_5 at 10 K using the ratio of $RRR_{CsV_3Sb_5}/RRR_{CsV_3(Sb_{0.977}As_{0.023})_5} = 4.13$, indicating that the functional form of MR remains unchanged in $CsV_3(Sb_{0.977}As_{0.023})_5$.

Figure 5(c) shows the field dependence of Hall resistivity (ρ_{xy}) at various temperatures. At low temperatures, the ρ_{xy} initially rises nonlinearly and then increases linearly at high magnetic fields. It is interesting that ρ_{xy} remains negative at every temperature, in contrast to sign reversal at around 30 K in CsV_3Sb_5 [24] even at 0.36 GPa [41]. A similar disappearance of the sign reversal in ρ_{xy} was reported in Nb-doped CsV_3Sb_5 [36]. The different behaviors of the Hall coefficient between $CsV_3(Sb_{0.977}As_{0.023})_5$ and CsV_3Sb_5 could be due to the significant decrease of hole-carrier mobility. The Hall resistivity can be described as below:

$$\rho_{xy} = \frac{\left(n_h\mu_h^2 - n_e\mu_e^2\right) + \mu_h^2\mu_e^2(n_h - n_e)B^2}{(n_e\mu_e - n_h\mu_h)^2 + \mu_h^2\mu_e^2(n_h - n_e)^2B^2}\frac{B}{e}, \qquad (2)$$

where n_e, n_h and μ_h, μ_h are the density and mobility of electrons and holes, respectively. Supposing the contrast between n_e and n_h is very small here, the Hall resistivity would be linearly dependent on field, as observed in experiments. Therefore, Hall resistivity could be simplified as $\rho_{xy} = \frac{1}{n}(\frac{2}{1+\mu_e/\mu_h} - 1)$. In CsV_3Sb_5, the mobility of the hole obtains a rapid increase at low temperature [3,24], which leads to a large positive ρ_{xy}. However, the mobility could be significantly suppressed by disorder, which is in accord with the sharp decrease in magnetoresistance. The ρ_{xy} becomes negative when μ_e/μ_h reaches above 1. Note that, in Nb-doped CsV_3Sb_5, sign reversal in ρ_{xy} disappears gradually as the doping level increases [36]. On the other hand, Li and Kato *et al.* [36,37] ascribe the vanishing of sign reversal to the antiphase shift of the Fermi energy with respect to M and Γ points.

Through the linear fit above the magnetic field of 2 T, the Hall coefficients (R_H) are extracted as shown in the inset. The R_H decreases gradually above T_{CDW} and then increases at low temperatures, generating a minimum at T_{CDW}. Compared with CsV_3Sb_5, the absolute value of R_H changes from $\sim 1.92 \times 10^{-4}$ to 2.39×10^{-4} cm^3 C^{-1} at 300 K [24]. The slight increase of R_H indicates a decrease of carrier density according to the single-band model. Figure 5(d) presents the AHE term observed below CDW after subtracting the local linear Hall part, which has the same magnitude as that reported in CsV_3Sb_5. The inset shows the temperature dependence of saturated ρ^{AHE}, defined as the mean value between 2 and 4 T. Indeed, the AHE gradually disappears at $T_{CDW} = 85$ K. The fact that the AHE appears simultaneously with the CDW transition suggests the intimate relationship between AHE and CDW.

IV. DISCUSSION AND CONCLUSION

Table I lists the physical parameters of CsV_3Sb_5 and $CsV_3(Sb_{0.977}As_{0.023})_5$. Although the As doping level is limited, there are still many significant differences. On the one hand, T_c is enhanced to 3.6 K from 2.5 K while T_{CDW} is suppressed from 94 to 83 K.The anticorrelation between SC and CDW clearly indicates their competitive relationship, as also revealed by the experiments of hydrostatic pressure. The doping level of 2.3% accounts for a hydrostatic pressure of 0.19 or 0.36 GPa with a close T_{CDW}, while T_c is slightly lower under hydrostatic pressure. The mechanism of SC enhancement in $CsV_3(Sb_{0.977}As_{0.023})_5$ is understood by both the pressure effect and the disorder effect. For the former case, it is interesting that the T_c values of RbV_3Sb_5 and KV_3Sb_5

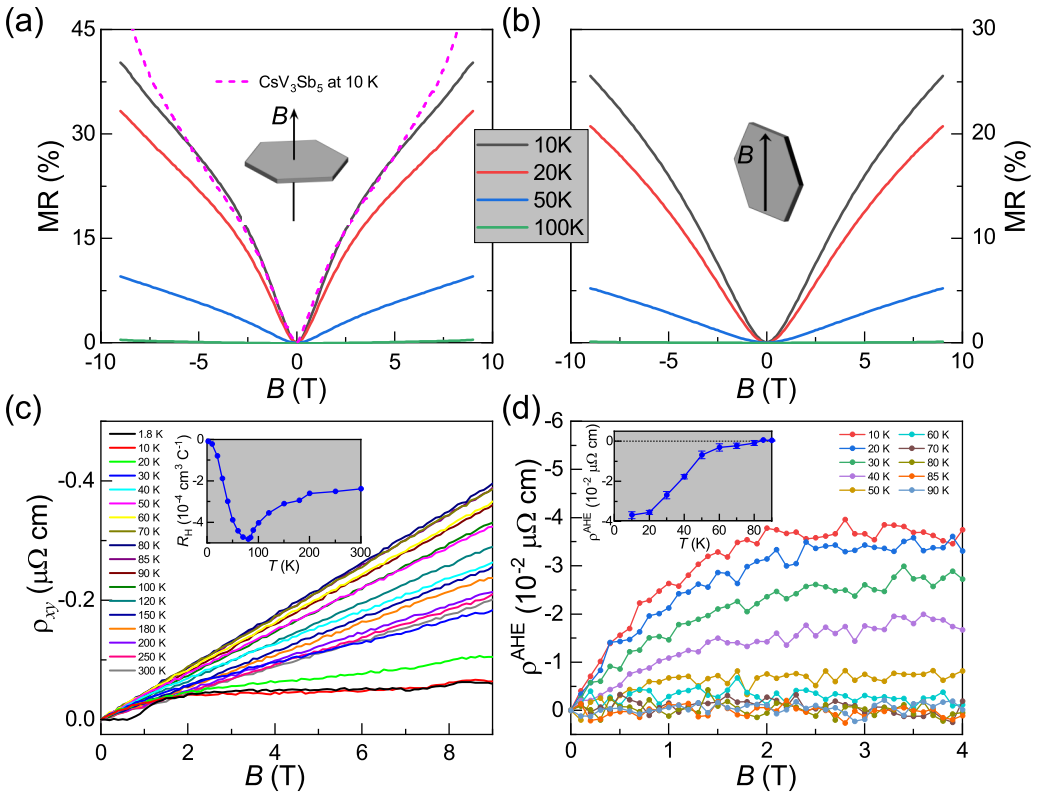

FIG. 5. Magnetoresistance measured at selected temperatures with field parallel (a) and perpendicular (b) to the c axis, respectively. The magenta dotted line is the magnetoresistance of CsV_3Sb_5 at 10 K after being divided by $RRR_{CsV_3Sb_5}/RRR_{CsV_3(Sb_{0.977}As_{0.023})_5}$. (c) Field dependence of Hall resistivity at selected temperatures with magnetic field up to 9 T. The inset shows the temperature dependence of the Hall coefficient. (d) The extracted ρ^{AHE} at different temperatures. The inset shows the temperature dependence of the saturated ρ^{AHE}.

are below 1 K, and their T_{CDW} values are 103 and 78 K, respectively. Therefore, isovalent substitutions at Cs sites and As sites have different effects. Only the As doping tends to generate a chemical pressure identical to the hydrostatic one. For the latter case, note that the CDW order is suppressed rapidly and T_c increases to 4.45 K with 7% Nb doping, indicating that the disorder effect of the isovalent substitution may also weaken CDW order and is benefit to SC. On the other hand, in $CsV_3(Sb_{0.977}As_{0.023})_5$, according to the McMillan equation, the electron-phonon coupling is strengthened from 0.62 to 0.72. The calculated Wilson ratio $R_W = \frac{1}{3}\frac{\pi k_B}{\mu_B}^2 \frac{\chi_P}{\gamma}$ for CsV_3Sb_5 and $CsV_3(Sb_{0.977}As_{0.023})_5$ is 1.4 and 1.5, respectively, indicating the slight enhancement of quasiparticle interactions, which is consistent with the increase of electron-phonon coupling. Another important parameter to estimate the correlation of quasiparticles is the Kadowaki-Woods ratio $R_{KW} = A/\gamma^2$, which is usually a constant for a certain class of materials. R_{KW} for CsV_3Sb_5 and $CsV_3(Sb_{0.977}As_{0.023})_5$ are 7.2 and 14.5 $\mu\Omega$ cm K^2 mol^2 J^{-2}. Cavanagh suggested that the Kadowaki-Woods ratio fails to measure the electronic correlations for multiband metals, which may be seriously affected by carrier density and impurity [46]. The doubling of R_{KW} in $CsV_3(Sb_{0.977}As_{0.023})_5$ is in agreement with the increase of impurity scattering and the decrease of carrier density.

TABLE I. Physical property parameters of CsV_3Sb_5 and $CsV_3(Sb_{0.977}As_{0.023})_5$. Conventional notations are employed, which can be found in the related text.

Parameters	CsV_3Sb_5	$CsV_3(Sb_{0.977}As_{0.023})_5$
c (Å)	9.328 [47]	9.313
T_c (K)	2.6	3.6
T_{CDW} (K)	94	83
$H_{c2}^{\perp}(T=0)$ (T)	0.8	1.1
$H_{c2}^{\parallel}(T=0)$ (T)	7.2	7.5
χ_P (10^{-4} emu mol^{-1} Oe^{-1})	3.6	3.3
γ (mJ K^{-2} mol^{-1})	20.03	16.77
θ_D (K)	174	153
A (nΩ cm K^{-2})	2.88	4.08
RRR	69	16

In summary, we have performed detailed physical property measurements on an As-doped CsV_3Sb_5 single crystal. It was found that only a small amount of Sb atoms (about 2.3%) can be substituted by As atoms in CsV_3Sb_5. In the $CsV_3(Sb_{0.977}As_{0.023})_5$ crystal, T_c is enhanced from 2.5 to 3.6 K and T_{CDW} is suppressed from 93 to 83 K simultaneously, which is basically consistent with the effect observed in the hydrostatic pressure study. The DOS deduced from Pauli paramagnetism decreases slightly, and the Sommerfeld coefficient is also reduced. It is interesting to ascertain whether the As atoms prefer Sb1 sites or Sb2 sites. In the case of Sn doping, the Sn atoms tend to stay in the kagome layers. The significant changes of physical properties with

the low-level doping suggest that As atoms could dominantly occupy the Sb1 site in the kagome plane. Further research, including transport measurements under higher magnetic fields, angle-resolved photoemission spectroscopy, and electronic structure calculations on As-doped CsV_3Sb_5, will be able to provide more information about this chemical pressure effect.

ACKNOWLEDGMENTS

This work was supported by the National Natural Science Foundation of China (Grants No. 12050003 and No. 12004337), the Key Research and Development Program of Zhejiang Province, China (Grant No. 2021C01002), and Zhejiang Provincial Natural Science Foundation of China (Grants No. LQ21A040011 and No. LQ19A040010).

[1] B. R. Ortiz, L. C. Gomes, J. R. Morey, M. Winiarski, M. Bordelon, J. S. Mangum, I. W. H. Oswald, J. A. Rodriguez-Rivera, J. R. Neilson, S. D. Wilson, E. Ertekin, T. M. McQueen, and E. S. Toberer, New kagome prototype materials: discovery of KV_3Sb_5, RbV_3Sb_5, and CsV_3Sb_5, Phys. Rev. Mater. **3**, 094407 (2019).

[2] B. R. Ortiz, P. M. Sarte, E. M. Kenney, M. J. Graf, S. M. L. Teicher, R. Seshadri, and S. D. Wilson, Superconductivity in the $\mathbb{Z}_2$ kagome metal KV_3Sb_5, Phys. Rev. Mater. **5**, 034801 (2021).

[3] Q. Yin, Z. Tu, C. Gong, Y. Fu, S. Yan, and H. Lei, Superconductivity and normal-state properties of kagome metal RbV_3Sb_5 single crystals, Chin. Phys. Lett. **38**, 037403 (2021).

[4] S. Ni, S. Ma, Y. Zhang, J. Yuan, H. Yang, Z. Lu, N. Wang, J. Sun, Z. Zhao, D. Li, S. Liu, H. Zhang, H. Chen, K. Jin, J. Cheng, L. Yu, F. Zhou, X. Dong, J. Hu, H.-J. Gao *et al.*, Anisotropic superconducting properties of kagome metal CsV_3Sb_5, Chin. Phys. Lett. **38**, 057403 (2021).

[5] Y.-X. Jiang, J.-X. Yin, M. M. Denner, N. Shumiya, B. R. Ortiz, G. Xu, Z. Guguchia, J. He, M. S. Hossain, X. Liu, J. Ruff, L. Kautzsch, S. S. Zhang, G. Chang, I. Belopolski, Q. Zhang, T. A. Cochran, D. Multer, M. Litskevich, Z.-J. Cheng *et al.*, Unconventional chiral charge order in kagome superconductor CsV_3Sb_5, Nat. Mater. **20**, 1353 (2021).

[6] N. Shumiya, M. S. Hossain, J.-X. Yin, Y.-X. Jiang, B. R. Ortiz, H. Liu, Y. Shi, Q. Yin, H. Lei, S. S. Zhang, G. Chang, Q. Zhang, T. A. Cochran, D. Multer, M. Litskevich, Z.-J. Cheng, X. P. Yang, Z. Guguchia, S. D. Wilson, and M. Z. Hasan, Intrinsic nature of chiral charge order in the kagome superconductor RbV_3Sb_5, Phys. Rev. B **104**, 035131 (2021).

[7] Z. Liang, X. Hou, F. Zhang, W. Ma, P. Wu, Z. Zhang, F. Yu, J.-J. Ying, K. Jiang, L. Shan, Z. Wang, and X.-H. Chen, Three-Dimensional Charge Density Wave and Surface-Dependent Vortex-Core States in a Kagome Superconductor CsV_3Sb_5, Phys. Rev. X **11**, 031026 (2021).

[8] Y.-P. Lin and R. M. Nandkishore, Complex charge density waves at Van Hove singularity on hexagonal lattices: Haldane-model phase diagram and potential realization in the kagome metals AV_3Sb_5 (A=K, Rb, Cs), Phys. Rev. B **104**, 045122 (2021).

[9] H. Tan, Y. Liu, Z. Wang, and B. Yan, Charge Density Waves and Electronic Properties of Superconducting Kagome Metals, Phys. Rev. Lett. **127**, 046401 (2021).

[10] E. Uykur, B. R. Ortiz, O. Iakutkina, M. Wenzel, S. D. Wilson, M. Dressel, and A. A. Tsirlin, Low-energy optical properties of the nonmagnetic kagome metal CsV_3Sb_5, Phys. Rev. B **104**, 045130 (2021).

[11] Z. Wang, S. Ma, Y. Zhang, H. Yang, Z. Zhao, Y. Ou, Y. Zhu, S. Ni, Z. Lu, H. Chen, K. Jiang, L. Yu, Y. Zhang, X. Dong, J. Hu, H.-J. Gao, and Z. Zhao, Distinctive momentum dependent charge-density-wave gap observed in CsV_3Sb_5 superconductor with topological kagome lattice, arXiv:2104.05556.

[12] M. M. Denner, R. Thomale, and T. Neupert, Analysis of Charge Order in the Kagome Metal AV_3Sb_5 (A = K, Rb, Cs), Phys. Rev. Lett. **127**, 217601 (2021).

[13] N. Ratcliff, L. Hallett, B. R. Ortiz, S. D. Wilson, and J. W. Harter, Coherent phonon spectroscopy and interlayer modulation of charge density wave order in the kagome metal CsV_3Sb_5, Phys. Rev. Mater. **5**, L111801 (2021).

[14] H. Chen, H. Yang, B. Hu, Z. Zhao, J. Yuan, Y. Xing, G. Qian, Z. Huang, G. Li, Y. Ye, S. Ma, S. Ni, H. Zhang, Q. Yin, C. Gong, Z. Tu, H. Lei, H. Tan, S. Zhou, C. Shen *et al.*, Roton pair density wave in a strong-coupling kagome superconductor, Nature (London) **599**, 222 (2021).

[15] J. Zhao, W. Wu, Y. Wang, and S. A. Yang, Electronic correlations in the normal state of the kagome superconductor KV_3Sb_5, Phys. Rev. B **103**, L241117 (2021).

[16] B. R. Ortiz, S. M. L. Teicher, Y. Hu, J. L. Zuo, P. M. Sarte, E. C. Schueller, A. M. Milinda Abeykoon, M. J. Krogstad, S. Rosenkranz, R. Osborn, R. Seshadri, L. Balents, J. He, and S. D. Wilson, CsV_3Sb_5: A $\mathbb{Z}_2$ Topological Kagome Metal with a Superconducting Ground State, Phys. Rev. Lett. **125**, 247002 (2020).

[17] W. Duan, Z. Nie, S. Luo, F. Yu, B. R. Ortiz, L. Yin, H. Su, F. Du, A. Wang, Y. Chen, X. Lu, J. Ying, S. D. Wilson, X. Chen, Y. Song, and H. Yuan, Nodeless superconductivity in the kagome metal CsV_3Sb_5, Sci. Chin.: Phys., Mech. Astron. **64**, 107462 (2021).

[18] C. Mu, Q. Yin, Z. Tu, C. Gong, H. Lei, Z. Li, and J. Luo, S-Wave superconductivity in kagome metal CsV_3Sb_5 revealed by $^{121/123}$Sb NQR and ^{51}V NMR measurements, Chin. Phys. Lett. **38**, 077402 (2021).

[19] H.-S. Xu, Y.-J. Yan, R. Yin, W. Xia, S. Fang, Z. Chen, Y. Li, W. Yang, Y. Guo, and D.-L. Feng, Multiband Superconductivity with Sign-Preserving Order Parameter in Kagome Superconductor CsV_3Sb_5, Phys. Rev. Lett. **127**, 187004 (2021).

[20] R. Gupta, D. Das, C. Mielke III, Z. Guguchia, T. Shiroka, C. Baines, M. Bartkowiak, H. Luetkens, R. Khasanov, Q. Yin, Z. Tu, G. Chunsheng, and H. Lei, Microscopic evidence for anisotropic multigap superconductivity in the CsV_3Sb_5 kagome superconductor, npj Quantum Mater. **7**, 49 (2022).

[21] E. M. Kenney, B. R. Ortiz, C. Wang, S. D. Wilson, and M. J. Graf, Absence of local moments in the kagome metal KV_3Sb_5 as determined by muon spin spectroscopy, J. Phys.: Condens. Matter **33**, 235801 (2021).

[22] M. Kang, S. Fang, J.-K. Kim, B. R. Ortiz, S. H. Ryu, J. Kim, J. Yoo, G. Sangiovanni, D. Di Sante, B.-G. Park, C. Jozwiak,

A. Bostwick, E. Rotenberg, E. Kaxiras, S. D. Wilson, J.-H. Park, and R. Comin, Twofold van Hove singularity and origin of charge order in topological kagome superconductor CsV_3Sb_5, Nat. Phys. **18**, 301 (2022).

[23] S.-Y. Yang, Y. Wang, B. R. Ortiz, D. Liu, J. Gayles, E. Derunova, R. Gonzalez-Hernandez, L. Smejkal, Y. Chen, S. S. P. Parkin, S. D. Wilson, E. S. Toberer, T. McQueen, and M. N. Ali, Giant, unconventional anomalous Hall effect in the metallic frustrated magnet candidate, KV_3Sb_5, Sci. Adv. **6**, eabb6003 (2020).

[24] F. H. Yu, T. Wu, Z. Y. Wang, B. Lei, W. Z. Zhuo, J. J. Ying, and X. H. Chen, Concurrence of anomalous Hall effect and charge density wave in a superconducting topological kagome metal, Phys. Rev. B **104**, L041103 (2021).

[25] F. Du, S. Luo, B. R. Ortiz, Y. Chen, W. Duan, D. Zhang, X. Lu, S. D. Wilson, Y. Song, and H. Yuan, Pressure-induced double superconducting domes and charge instability in the kagome metal KV_3Sb_5, Phys. Rev. B **103**, L220504 (2021).

[26] F. H. Yu, D. H. Ma, W. Z. Zhuo, S. Q. Liu, X. K. Wen, B. Lei, J. J. Ying, and X. H. Chen, Unusual competition of superconductivity and charge-density-wave state in a compressed topological kagome metal, Nat. Commun. **12**, 3645 (2021).

[27] K. Y. Chen, N. N. Wang, Q. W. Yin, Y. H. Gu, K. Jiang, Z. J. Tu, C. S. Gong, Y. Uwatoko, J. P. Sun, H. C. Lei, J. P. Hu, and J.-G. Cheng, Double Superconducting Dome and Triple Enhancement of T_c in the Kagome Superconductor CsV_3Sb_5 under High Pressure, Phys. Rev. Lett. **126**, 247001 (2021).

[28] Z. Zhang, Z. Chen, Y. Zhou, Y. Yuan, S. Wang, J. Wang, H. Yang, C. An, L. Zhang, X. Zhu, Y. Zhou, X. Chen, J. Zhou, and Z. Yang, Pressure-induced reemergence of superconductivity in the topological kagome metal CsV_3Sb_5, Phys. Rev. B **103**, 224513 (2021).

[29] X. Chen, X. Zhan, X. Wang, J. Deng, X.-B. Liu, X. Chen, J.-G. Guo, and X. Chen, Highly robust reentrant superconductivity in CsV_3Sb_5 under pressure, Chin. Phys. Lett. **38**, 057402 (2021).

[30] F. Du, R. Li, S. Luo, Y. Gong, Y. Li, S. Jiang, B. R. Ortiz, Y. Liu, X. Xu, S. D. Wilson, C. Cao, Y. Song, and H. Yuan, Superconductivity modulated by structural phase transitions in pressurized vanadium-based kagome metals, Phys. Rev. B **106**, 024516 (2022).

[31] T. Das and C. Panagopoulos, Two types of superconducting domes in unconventional superconductors, New J. Phys. **18**, 103033 (2016).

[32] Y. Song, T. Ying, X. Chen, X. Han, X. Wu, A. P. Schnyder, Y. Huang, J.-g. Guo, and X. Chen, Competition of Superconductivity and Charge Density Wave in Selective Oxidized CsV_3Sb_5 Thin Flakes, Phys. Rev. Lett. **127**, 237001 (2021).

[33] H. Yang, Y. Zhang, Z. Huang, Z. Zhao, J.-a. Shi, G. Qian, H. Bin, Z. Lu, H. Zhang, C. Shen, X. Lin, Z. Wang, S. Pennycook, H. Chen, X. Dong, W. Zhou, and H.-J. Gao, Titanium doped kagome superconductor CsV_3-xTixSb_5 and two distinct phases, arXiv:2110.11228.

[34] Y. M. Oey, B. R. Ortiz, F. Kaboudvand, J. Frassineti, E. Garcia, R. Cong, S. Sanna, V. F. Mitrović, R. Seshadri, and S. D. Wilson, Fermi level tuning and double-dome superconductivity in the kagome metal $CsV_3Sb_{5-x}Sn_x$, Phys. Rev. Mater. **6**, L041801 (2022).

[35] H. LaBollita and A. S. Botana, Tuning the Van Hove singularities in AV_3Sb_5(A = K, Rb, Cs) via pressure and doping, Phys. Rev. B **104**, 205129 (2021).

[36] Y. Li, Q. Li, X. Fan, J. Liu, Q. Feng, M. Liu, C. Wang, J.-X. Yin, J. Duan, X. Li, Z. Wang, H.-H. Wen, and Y. Yao, Tuning the competition between superconductivity and charge order in the kagome superconductor $Cs(V_{1-x}Nb_x)_3Sb_5$, Phys. Rev. B **105**, L180507 (2022).

[37] T. Kato, Y. Li, K. Nakayama, Z. Wang, S. Souma, F. Matsui, M. Kitamura, K. Horiba, H. Kumigashira, T. Takahashi, Y. Yao, and T. Sato, Fermiology and origin of T_c enhancement in a kagome superconductor $Cs(V_{1-x}Nb_x)_3Sb_5$, Phys. Rev. Lett. **129**, 206402 (2022).

[38] Z. Ren, Q. Tao, S. Jiang, C. Feng, C. Wang, J. Dai, G. Cao, and Z. Xu, Superconductivity Induced by Phosphorus Doping and Its Coexistence with Ferromagnetism in $EuFe_2(As_{0.7}P_{0.3})_2$, Phys. Rev. Lett. **102**, 137002 (2009).

[39] F. Yu, X. Zhu, X. Wen, Z. Gui, Z. Li, Y. Han, T. Wu, Z. Wang, Z. Xiang, Z. Qiao, J. Ying, and X. Chen, Pressure-Induced Dimensional Crossover in a Kagome Superconductor, Phys. Rev. Lett. **128**, 077001 (2022).

[40] The susceptibility in the Pauli paramagnetic state is contributed by the serval terms, namely $\chi = \chi_P + \chi_L + \chi_{core} + \chi_V$. χ_P is the Pauli susceptibility, and the other three terms are susceptibility from Landau diamagnetism, atomic-core diamagnetism, and van Vleck paramagnetism separately. We only consider χ_P here, and the other three terms are ignored

[41] F.-H. Yu, X.-K. Wen, Z.-G. Gui, T. Wu, Z. Wang, Z.-J. Xiang, J. Ying, and X. Chen, Pressure tuning of the anomalous Hall effect in the kagome superconductor CsV_3Sb_5, Chin. Phys. B **31**, 017405 (2022).

[42] A. Gurevich, Enhancement of the upper critical field by nonmagnetic impurities in dirty two-gap superconductors, Phys. Rev. B **67**, 184515 (2003).

[43] The upper critical field [$H_{c2}(0)$] is related to Ginzburg-Landau coherence length (ξ_{GL}) with the equation $\xi_{GL} = \sqrt{\frac{\Phi_0}{2\pi H_{c2}(0)}}$, where Φ_0 is the flux quantum. ξ_{GL} is proportional to the mean free path (l) with the relation $\xi_{GL} = \sqrt{\xi_{BCS} l}$, where ξ_{BCS} is the BCS coherence length. Therefore, a decrease of l usually leads to an increase of $H_{c2}(0)$.

[44] W. L. McMillan, Transition temperature of strong-coupled superconductors, Phys. Rev. **167**, 331 (1968).

[45] Y. Zhong, S. Li, H. Liu, Y. Dong, Y. Arai, H. Li, Y. Shi, Z. Wang, S. Shin, H. N. Lee, H. Miao, T. Kondo, and K. Okazaki, Testing electron-phonon coupling for the superconductivity in kagome metal CsV_3Sb_5, arXiv:2207.02407.

[46] D. C. Cavanagh, A. C. Jacko, and B. J. Powell, Breakdown of the universality of the Kadowaki-Woods Ratio in multi-band metals, Phys. Rev. B **92**, 195138 (2015).

[47] This parameter is calculated from the data shown in Fig. 1(c).